

# A Characteristic Wind Signature in Prompt GRB Afterglows

Shiho Kobayashi<sup>1,2</sup>, Peter Mészáros<sup>1,2</sup> and Bing Zhang<sup>1</sup>

<sup>1</sup>*Department of Astronomy & Astrophysics, Pennsylvania State University, University Park, PA 16802*

<sup>2</sup>*Center for Gravitational Wave Physics, Pennsylvania State University, University Park, PA 16802*

## ABSTRACT

We discuss the self-absorption effects in the prompt emission from the reverse shock in GRB afterglows that occur in the wind environment of a massive stellar progenitor. We point out that the higher self-absorption frequency in a wind environment implies a hump in the reverse shock emission spectrum and a more complex optical/IR light curve behavior than previously thought. We discuss a possible new diagnostic to test for the presence of a wind environment, and to provide constraints on the progenitor wind mass loss and the burst parameters.

## 1. Introduction

The prompt optical flashes detected seconds to minutes after the gamma-ray trigger in several GRB afterglows (Akerlof et al., 1999; Fox et al. 2003a; Fox et al. 2003b; Li et al. 2003) have been attributed to the emission from the reverse shock (e.g., Sari & Piran, 1999; Mészáros & Rees 1999; Kobayashi 2000; Kobayashi & Zhang 2003a). The reverse shock, which lasts typically for a short time, tends to be in the regime where the electron cooling time is shorter than the dynamical expansion time, and the characteristic cooling frequency (Sari, Piran & Narayan, 1998), which is density dependent, plays a role in determining the prompt reverse shock flux and light curve behavior (Kobayashi & Zhang 2003b).

Snapshot fits of the broadband spectrum of afterglows to standard forward shock models have been found, in many cases, to be consistent with an external environment density  $n \lesssim 1 \text{ cm}^{-3}$  typical of a dilute interstellar medium (ISM) which, to first order, can be taken to be approximately independent of distance from the burst (Frail et al 2001). In other cases, the forward shock is better fitted with an external density which depends on distance as  $\rho \propto R^{-2}$ , typical of a stellar wind environment (Chevalier & Li 1999, 2000; Li & Chevalier 2003). The two types of fits have been critically analyzed by e.g., Panaiteescu and Kumar (2002), the conclusion being that at least some bursts may occur in high mass-loss winds, as

expected from massive progenitors. The parameters for such wind fits are uncertain, due to poorly known stellar mass loss rates.

In this Letter we concentrate on the properties of the afterglow reverse shock in a stellar wind environment. Whereas in a typical ISM external medium the reverse shock self-absorption frequency is generally below the cooling frequency, in wind environments the density is higher, and the self-absorption frequency is generally higher than the cooling frequency (Wu et al. 2003). Here we argue, from general radiative transfer considerations, that in such situations when the self-absorption frequency exceeds the cooling frequency, the absorption frequency and its scaling is different, and the flux at the absorption frequency is appreciably larger than what had been previously estimated for winds. This also implies a different light curve time behavior for the wind afterglow prompt flash. In view of recent evidence in favor of a massive progenitor, this is of significant interest, since it provides a new diagnostic for the presence of a wind, and a possible constraint on the otherwise poorly known wind mass-loss rates of progenitor stars (since both the self-absorption frequency and the net flux depend on the wind density). It is also relevant in view of the significant interest attached to studies of prompt flashes from reverse shocks, e.g. with *Swift*, as a tool to investigate the early afterglow dynamics, and the transition from the prompt shock to the external shock phase.

## 2. The Model

We consider a relativistic shell (fireball ejecta) with an isotropic energy  $E$ , an initial Lorentz factor  $\eta$  and an initial width  $\Delta_0$  expanding into a surrounding medium with a density distribution  $\rho = AR^{-2}$ . The shell width  $\Delta_0$  is related to the intrinsic duration of the GRB as  $\Delta_0 \sim (1+z)^{-1}cT$  (Kobayashi, Piran & Sari 1997) where  $z$  is the redshift of the burst. The interaction between the shell and the wind is described by two shocks: a forward shock propagating into the wind and a reverse shock propagating into the shell. The shocks accelerate electrons in the shell and in the wind material, and the electrons emit photons via synchrotron process.

The evolution of the reverse shocks can be classified into two cases depending on the value of the initial bulk Lorentz factor  $\eta$  relative to a critical Lorentz factor  $\eta_{cr} = ((1+z)E/4\pi Ac^3T)^{1/4}$  (Sari & Piran 1995; Kobayashi & Zhang 2003b). If  $\eta > \eta_{cr}$  (thick-shell case), the reverse shock is relativistic from the beginning and it significantly decelerates the shell material  $\Gamma \sim \eta_{cr}$ . The shock crosses the shell at a time  $t_x$  comparable to the GRB duration  $T$ . If  $\eta < \eta_{cr}$  (thin-shell case), the reverse shock is initially Newtonian and becomes only mildly relativistic when it traverses the shell at  $t_x \sim (\eta_{cr}/\eta)^4T > T$ . Most bursts in

a wind environment fall in the classification of thick-shell case ( $\eta > \eta_{cr}$ ), because the high density makes the critical Lorentz factor  $\eta_{cr} \sim 40 \zeta^{1/4} E_{52}^{1/4} A_{11.7}^{-1/4} T_{50}^{-1/4}$  lower than the value required by the fireball model  $\Gamma \gtrsim 100$  (e.g., Lithwick & Sari 2001), where  $\zeta = (1+z)/2$ ,  $E_{52} = E/10^{52}$  ergs, the duration  $T_{50} = T/50$  sec, and  $A_{11.7} = A/5 \times 10^{11}$  g cm<sup>-1</sup> is a typical wind mass loss rate. We are especially interested in long bursts with  $t_x \gtrsim$  a minute for the purpose of analyzing the light curve behavior of the reverse shock emission. We focus the discussion on the thick-shell case, for which one can take the shock crossing time  $t_x \sim T$  and the value of the bulk Lorentz factor during the shock crossing ( $t < t_x$ ) is  $\Gamma \sim \eta_{cr}$ .

If we neglect the synchrotron self-absorption (which will be discussed in the next section) the spectrum of the reverse shock is described by a broken power law with a peak  $F_{\nu,max}$  and two break frequencies: a typical frequency  $\nu_m$  and a cooling frequency  $\nu_c$  (Sari, Piran & Narayan 1998). Assuming that constant fractions ( $\epsilon_e$  and  $\epsilon_B$ ) of the internal energy produced by the shock go into the electrons and the magnetic field, the reverse shock spectrum at a shock crossing time  $t_x \sim T$  is characterized by (Kobayashi & Zhang 2003b),

$$\nu_c(T) \sim 1.5 \times 10^{12} \zeta^{-3/2} \epsilon_{B,-2}^{-3/2} E_{52}^{1/2} A_{11.7}^{-2} T_{50}^{1/2} \text{ Hz} \quad (1)$$

$$\nu_m(T) \sim 5.0 \times 10^{14} \zeta^{-1/2} \epsilon_{e,-1}^2 \epsilon_{B,-2}^{1/2} E_{52}^{-1/2} A_{11.7} \eta_2^2 T_{50}^{-1/2} \text{ Hz} \quad (2)$$

$$F_{\nu,max}(T) \sim 3.0 d^{-2} \zeta^2 \epsilon_{B,-2}^{1/2} E_{52} A_{11.7}^{1/2} \eta_2^{-1} T_{50}^{-1} \text{ Jy} \quad (3)$$

where  $\epsilon_{B,-2} = \epsilon_B/0.01$ ,  $\epsilon_{e,-1} = \epsilon_e/0.1$ ,  $\eta_2 = \eta/100$ ,  $d = d_L(z)/(2 \times 10^{28} \text{ cm})$ ,  $d_L(z)$  is the luminosity distance of the burst, and  $d_L(1) \sim 2 \times 10^{28} \text{ cm}$  for the standard cosmological parameters ( $\Omega_m = 0.3$ ,  $\Omega_\Lambda = 0.7$  and  $h = 0.7$ ),

### 3. Self-absorption

Since the wind density at the initial interaction with the shell is much larger than the medium density in the ISM model, the cooling frequency  $\nu_c$  is much lower than the typical (injection) frequency  $\nu_m$  in the wind model. Furthermore, the synchrotron self-absorption frequency  $\nu_{sa}$  is much higher than in the ISM model, and it is comparable to the typical frequency  $\nu_m$  at the shock crossing time:  $\nu_c(T) < \nu_{sa}(T) \lesssim \nu_m(T)$  (Kobayashi & Zhang 2003b). Therefore, self-absorption prevents electrons from cooling down to the Lorentz factor  $\gamma_c$  corresponding to the cooling frequency  $\nu_c$ , and the electrons injected at the shock pile up at the Lorentz factor  $\gamma_{sa}$  corresponding to the self-absorption frequency  $\nu_{sa}$ . This pile-up of electrons at  $\gamma_{sa}$  can lead to a distinctive hump in the spectrum of the wind reverse shock emission, providing a unique signature of the wind environment.

A simple estimate of the maximal self-absorption flux is the emission from the black body with the reverse shock temperature (e.g., Sari & Piran 1999; Chevalier & Li 2000). We

write this as

$$F_\nu^{bb} = 2\pi(1+z)\nu^2 m_e \eta_{cr} \gamma_{sa} \left( \frac{R_\perp}{d_L} \right)^2 \quad (4)$$

where  $R_\perp \sim 2\eta_{cr}cT$  is the observed size of the shell and  $\gamma_{sa}$  is the random Lorentz factor of electrons radiating at the self-absorption frequency  $\nu_{sa} = \eta_{cr}\gamma_{sa}^2 q_e B / 2\pi m_e c$ ,  $m_e$  and  $q_e$  are the mass and charge of electrons, respectively,  $B = (32\pi\epsilon_B\eta_{cr}^2\rho c^2)^{1/2}$  is the comoving magnetic field strength behind the shock, and for a thick shell,  $\Gamma \sim \eta_{cr}$  and  $t_x \sim T$ .

On the other hand, the flux of the synchrotron emission at a frequency  $\nu$  is proportional to  $N_e(\nu)B\Gamma$  where  $N_e(\nu)$  is the number of electrons emitting photons at the frequency  $\nu$ . Since almost all electrons in the shell have the random Lorentz factor  $\gamma_{sa}$ , the flux at  $\nu_{sa}$  should be equal to  $F_{\nu,max}$  given by eq. (3). Using the equality  $F_{\nu_{sa}}^{bb} \sim F_{\nu,max}$ , we obtain the self-absorption frequency.

$$\nu_{sa}(T) \sim 2.0 \times 10^{14} \zeta^{3/10} \epsilon_{B,-2}^{3/10} E_{52}^{1/10} A_{11.7}^{3/5} \eta_2^{-2/5} T_{50}^{-11/10} \text{ Hz.} \quad (5)$$

At the shock crossing time  $t_x \sim T$ , the flux at  $\nu_{sa}$  is larger by a factor of  $\sim (\nu_{sa}/\nu_c)^{1/2} \sim 10 \zeta^{9/10} \epsilon_{B,-2}^{9/10} E_{52}^{-1/5} A_{11.7}^{13/10} \eta_2^{-1/5} T_{50}^{-4/5}$  than the previously assumed values. The black-body flux at frequencies below the  $\nu_{sa}$  peak is also larger than previously assumed, by the same factor  $\sim (\nu_{sa}/\nu_c)^{1/2}$  (see fig 1).

The scalings of the spectral quantities at  $t < t_x$  are (Kobayashi & Zhang 2003b)

$$\nu_c \propto t, \quad \nu_{sa} \propto t^{-1}, \quad \nu_m \propto t^{-1}, \quad F_{\nu,max} \propto t^0. \quad (6)$$

where the scaling of  $\nu_{sa}$  was derived by using the same method presented by Kobayashi & Zhang (2003b). Although  $\nu_c$  itself is not observed, as a result of the self-absorption, the flux at  $\nu \gtrsim \nu_{sa}$  can be still estimated using these scalings, because the electron distribution  $N_e$  producing some observed frequency  $\nu$  (say at the R-band  $\nu_R > \nu_{sa}$ ) (and frequencies above this) is determined by the distribution of injected electrons at the shock, and by the synchrotron radiation cooling. Therefore, even though the flux at  $\nu_{sa}$  has a hump which was previously unaccounted for, we can apply the conventional synchrotron model to estimate the light curve at a frequency  $\nu \gtrsim \nu_{sa}$ .

The optical luminosity initially increases as  $\sim (\nu/\nu_{sa})^2 F_{\nu,max} \propto t^2$ . When the self-absorption frequency  $\nu_{sa} \propto t^{-1}$  passes through the optical R-band at  $t_{sa}$ , the flux reaches a peak of  $F_{\nu_R}(t_{sa}) \sim F_{\nu,max}$ , and then it rapidly decreases by a factor of  $\mathcal{R} \sim [\nu_{sa}(t_{sa})/\nu_c(t_{sa})]^{1/2}$ . At this turnover, a drastic color change from blue to red is expected (see fig 1).

$$t_{sa} \sim 20 \zeta^{3/10} \epsilon_{B,-2}^{3/10} E_{52}^{1/10} A_{11.7}^{3/5} \eta_2^{-2/5} T_{50}^{-1/10} \nu_{R,14.7}^{-1} \text{ sec,} \quad (7)$$

$$\mathcal{R} \sim 30 \zeta^{3/5} \epsilon_{B,-2}^{3/5} E_{52}^{-3/10} A_{11.7}^{7/10} \eta_2^{1/5} T_{50}^{3/10} \nu_{R,14.7} \quad (8)$$

where  $\nu_{R,14.7} = \nu_R/5 \times 10^{14}\text{Hz}$ . After the emission drops to the level expected from the usual synchrotron model, the flux slowly increases as  $\sim (\nu_R/\nu_c)F_{\nu,max} \sim t^{1/2}$ . After a timescale comparable to the burst duration  $T$ , the (reverse shock) optical emission fades rapidly, because no further electrons are being shocked in the shell (allowing the initially weaker but longer lasting forward shock component to gradually dominate). The angular time delay effect prevents the abrupt disappearance of the reverse component, whose flux decreases as  $\sim t^{-3}$  (Kobayashi & Zhang 2003b). No color change is expected around this second peak. The second peak flux value is given by

$$F_{\nu_R}(T) \sim 0.2 d^{-2} \zeta^{5/4} \epsilon_{B,-2}^{-1/4} E_{52}^{5/4} A_{11.7}^{-1/2} \nu_{R,14.7}^{-1/2} \eta_2^{-1} T_{50}^{-3/4} \text{ Jy} \quad (9)$$

These two peaks are schematically shown in Fig. 2, the sharp breaks being an idealization; in reality these would appear rounded.

In a wind-regime afterglow, the prompt detection of the two reverse shock peaks, with timescales and fluxes  $(t_{sa}, F_{\nu_R}(t_{sa}))$  and at  $(T, F_{\nu_R}(T))$ , would enable a determination of the wind mass loss rate  $A$ , the initial bulk Lorentz factor  $\eta$  and the magnetic equipartition factor  $\epsilon_B$ . This assumes that the redshift  $z$  has been measured, and that the explosion energy  $E$  of the GRB is determined, e.g. from late time bolometric afterglow observations. In this case, using eqs. (3), (7) and (9), we obtain

$$A \sim 5 \times 10^{11} d^{-3} \zeta^{9/4} E_{52} \nu_{R,14.7}^4 T_{50}^{-5/4} t_{sa,20}^{15/4} F_T^{1/2} F_{t_{sa}}^{-2} \text{ g cm}^{-1}, \quad (10)$$

$$\eta \sim 10^2 d^{-3/2} \zeta^{9/8} E_{52} \nu_{R,14.7}^{-1} T_{50}^{-5/8} t_{sa,20}^{-5/8} F_T^{-3/4}, \quad (11)$$

$$\epsilon_B \sim 10^{-2} d^4 \zeta^{-4} E_{52}^{-1} \nu_{R,14.7}^{-6} T_{50}^2 t_{sa,20}^{-5} F_T^{-2} F_{t_{sa}}^4, \quad (12)$$

where  $t_{sa,20} = t_{sa}/20$  sec,  $F_T = F_{\nu_R}(T)/0.2$  Jy,  $F_{t_{sa}} = F_{\nu_R}(t_{sa})/3$  Jy,  $\zeta = (1+z)/2$  and  $d = d_L(z)/(2 \times 10^{28}\text{cm})$ .

#### 4. Discussion and Conclusions

We have analyzed the prompt afterglow fluxes from the reverse shock of GRB which occurs in the dense stellar wind environment produced by their massive progenitor. We have pointed out that the usual prescription of normalizing the maximum synchrotron flux  $F_{\nu,max}$  by taking most of the electrons to have cooled to an energy  $\gamma_c$ , when the estimated  $\gamma_c$  is lower than the energy  $\gamma_{sa}$  of electrons emitting at the self-absorption frequency, should be inapplicable for estimating the flux at and below the self-absorption frequency. This is because re-absorption causes the cooling electrons to pile up at the absorption energy. Such conditions occur in the afterglow reverse shock in a wind, and hence the characteristic energy of the electrons responsible for the synchrotron peak is higher than the commonly

assumed equilibrium cooling Lorentz factor. The observer frame specific flux at the peak  $F_{\nu, \text{max}} \propto B^2 \gamma^2 \Gamma^2 / B \gamma^2 \Gamma \propto B \Gamma$ , where  $\Gamma$  is bulk Lorentz factor and  $B$  is comoving field, is independent of the electron random Lorentz factor  $\gamma$ , hence the flux at  $\nu_{sa}(\gamma_{sa})$  is the same as that previously ascribed to  $\nu_c(\gamma_c)$  (and it is higher by  $(\nu_{sa}/\nu_c)^{1/2}$  relative to previous estimates obtained using the scaling  $F_\nu \propto \nu^{-1/2}$  between  $\nu_c$  to  $\nu_{sa}$ ). As a result, the self-absorption frequency is different and scales differently with the shock parameters, and the specific flux at the self-absorption frequency shows a hump which is a factor  $(\nu_{sa}/\nu_c)^{1/2} \sim 30$  above the usual power law flux estimate for typical parameters. The flux well above  $\nu_{sa}$  is the same as before, but the flux below  $\nu_{sa}$  is larger by the same factor  $(\nu_{sa}/\nu_c)^{1/2} \sim 30$ . This results in a new type of temporal behavior for the prompt optical flash in wind afterglows, characterized by two peaks.

Massive stars appear implicated in producing long gamma-ray bursts (as seen from the detection of a supernova associated with GRB 030329, e.g., Stanek et al 2003). Wind mass loss is expected from such stars previous to the GRB explosion, but snapshot fits to forward shock late emission (e.g., Panaiteescu & Kumar, 2002) are compatible with such wind mass loss in only a handful of cases. In general the parameters of stellar winds are poorly known, and the uncertainties are further increased at high redshifts, where massive stars are expected to be metal poor. For this reason, unambiguous signatures of a wind mass loss would be extremely valuable, both for GRB astrophysics and for tracing the properties of star formation at high redshifts. The prompt optical flashes expected after tens of seconds from the reverse shock give, in a stellar wind environment, characteristic signatures in the spectral and temporal behavior, which may help to test for the presence of winds and determine both the wind mass loss and crucial parameters of the burst explosion. Future missions such as *Swift* complemented by ground-based follow-ups, geared towards detecting prompt afterglows in large numbers, should be able to detect such wind signatures and trace any changes with redshifts, if they are exist, and constrain the GRB environment as well as the radiation mechanisms.

This work is supported by NASA NAG5-13286 and the Pennsylvania State University Center for Gravitational Wave Physics, funded by NSF under cooperative agreement PHY 01-14375.

## References

Akerlof,C, et al. 1999, *Nature*, 398, 400.  
Chevalier,R.A. & Li,Z.Y. 1999, *ApJ*, 520, L29.  
Chevalier,R.A. & Li,Z.Y. 2000, *ApJ*, 536, 195.  
Fox,D.W. et al. 2003a, *Nature*, 422, 284.  
Fox,D.W. et al. 2003b, *ApJ*, 586, L5.  
Frail, D.A. et al. 2001, *ApJ*, 562, L55.  
Kobayashi,S. 2003, *ApJ*, 589, 861.  
Kobayashi,S, Piran,T. & Sari,R. 1997, *ApJ*, 490, 92.  
Kobayashi,S & Zhang,B. 2003a, *ApJ*, 582, L75.  
Kobayashi,S & Zhang,B. 2003b, *ApJ* in press, astro-ph/0304086.  
Li, W. et al. 2003, *ApJ*, 586, L9.  
Li,Z.Y. & Chevalier,R.A. 2003, *ApJ*, 589, L69.  
Lithwick,Y & Sari, R. 2001, *ApJ*, 555, 540.  
Mészáros , P. & Rees,M. 1999, *MNRAS*, 306, L39.  
Panaiteescu,A. & Kumar, P. 2002, *ApJ*, 571, 779.  
Sari,R. & Piran,T. 1995, *ApJ*, 455, L143.  
Sari,R. & Piran,T. 1999, *ApJ*, 517, L109.  
Sari,R., Piran,T. & Narayan,R. 1998, *ApJ*, 497, L17.  
Stanek,K.Z. et al. 2003, *ApJ*, 591, L17.  
Wu,X.F. et al. 2003, *MNRAS*, 342, 1131.

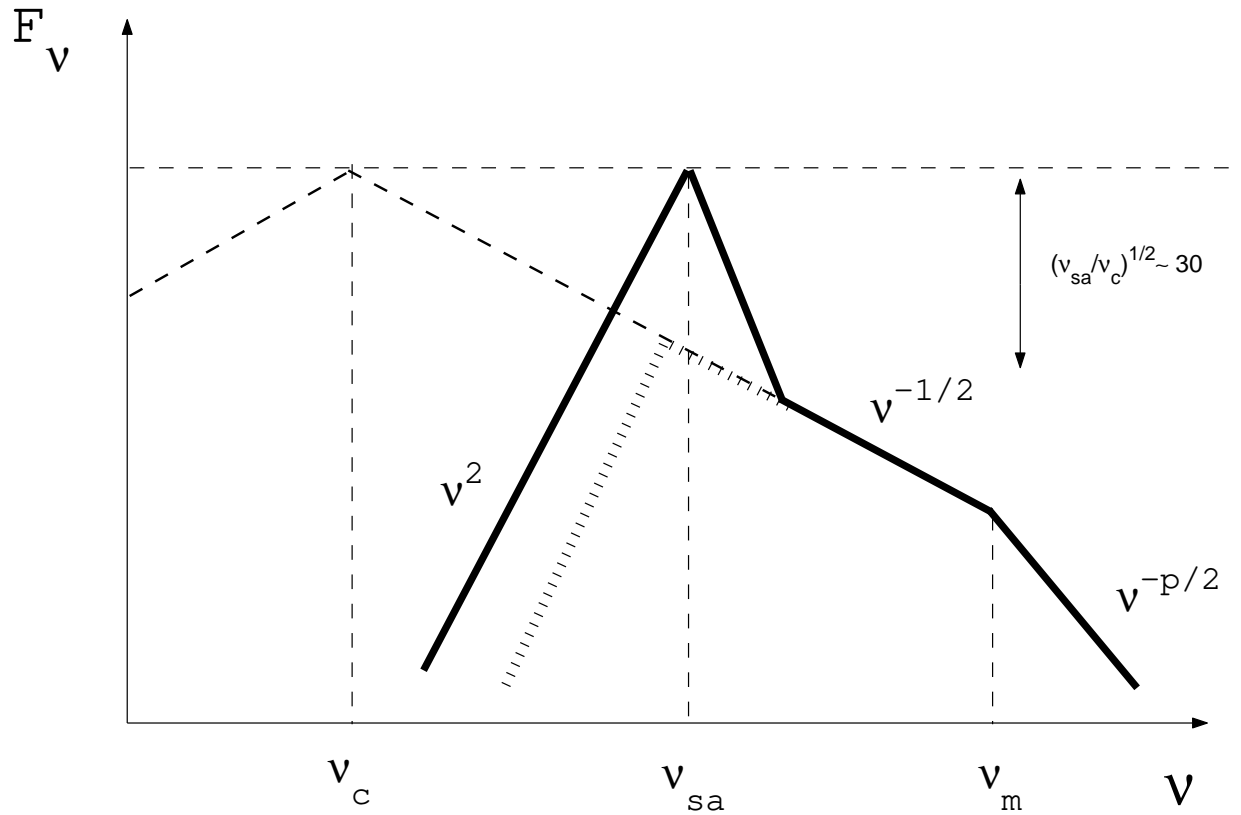


Fig. 1.— Wind reverse shock spectrum: with self-absorption (thick solid) and without self-absorption (thin dashed). The schematic self-absorption maximum would appear as a rounded thermal peak. The previous self-absorbed flux estimate is shown by hashed lines. The correction factor  $(\nu_{sa}/\nu_c)^{1/2} \propto t^{-1}$  is larger at earlier times ( $t < t_{\times}$ ), the value of  $\sim 30$  is evaluated at  $t_{sa}$  for typical parameters.

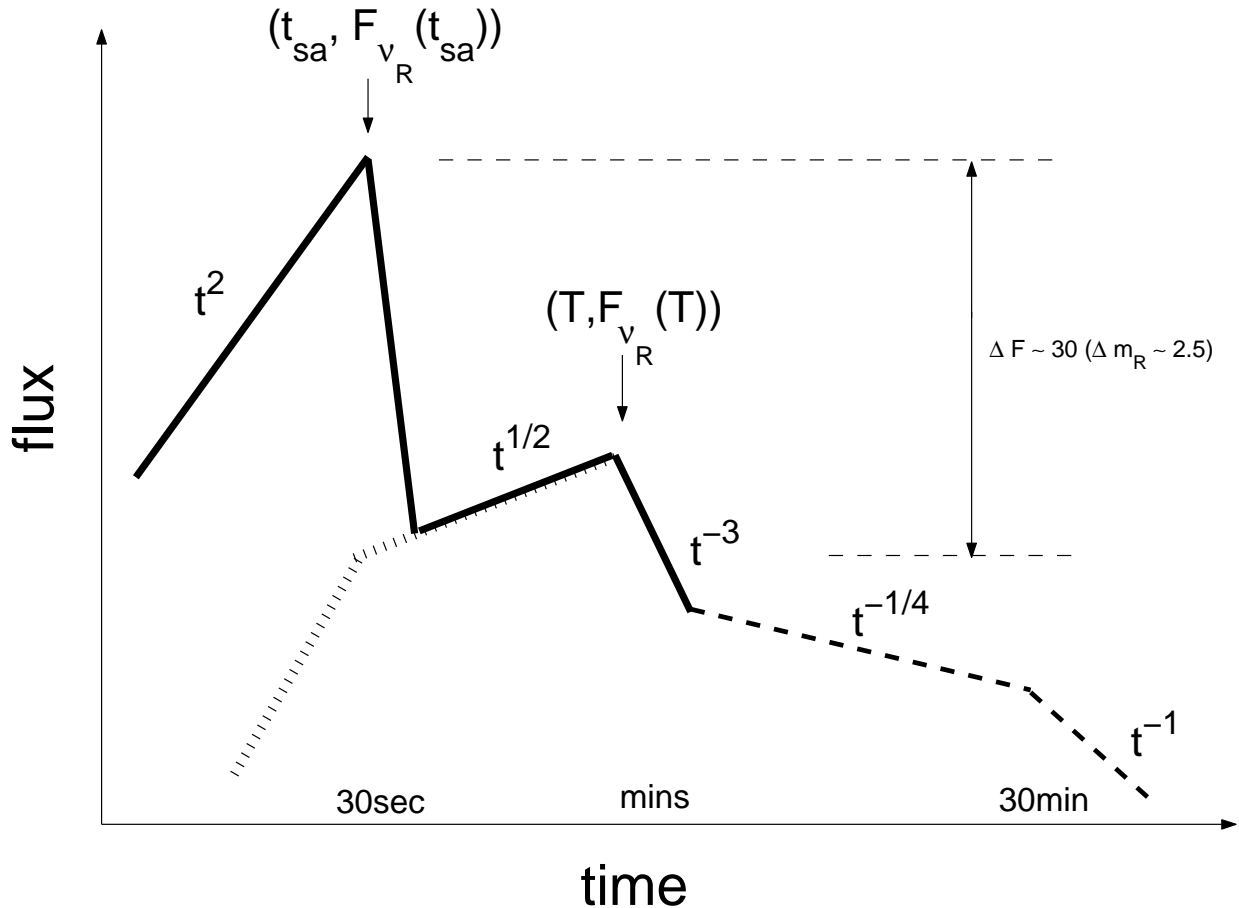


Fig. 2.— Schematic optical light curve in a wind environment: reverse shock emission (solid) and forward shock emission (dashed). The hashed line shows a previous estimate. Time scales are rough estimates for the typical parameters.